Cork Open Research Archive
Cartlann Taighde Oscailte Chorcaí

UCC Library and UCC researchers have made this item openly available. Please let us know how this has helped you. Thanks!

Title	Wireless pressure sensor using laser targeting of silicon carbide
Author(s)	Riza, Nabeel A.; Ghauri, Farzan N.; Perez, Frank
Publication date	2007-01-01
Original citation	Riza, N. A., Ghauri, F. N. and Perez, F. (2007) 'Wireless pressure sensor using laser targeting of silicon carbide', Optical Engineering 46(1), 014401 (9 pp). doi: 10.1117/1.2432885
Type of publication	Article (peer-reviewed)
Link to publisher's version	http://dx.doi.org/10.1117/1.2432885 Access to the full text of the published version may require a subscription.
Rights	© 2007 Society of Photo-Optical Instrumentation Engineers (SPIE). One print or electronic copy may be made for personal use only. Systematic reproduction and distribution, duplication of any material in this paper for a fee or for commercial purposes, or modification of the content of the paper are prohibited.
Item downloaded from	http://hdl.handle.net/10468/10044

University College Cork, Ireland
Coláiste na hOllscoile Corcaigh

Wireless pressure sensor using laser targeting of silicon carbide

Nabeel A. Riza
Nuonics, Inc.
1025 South Semoran Boulevard, Suite 1093
Winter Park, Florida 32792
    and
University of Central Florida
College of Optics-CREOL
4000 Central Florida Boulevard
Orlando, Florida 32816-2700

Farzan Ghauri
University of Central Florida
College of Optics-CREOL
4000 Central Florida Boulevard
Orlando, Florida 32816-2700

Frank Perez
Nuonics, Inc.
1025 South Semoran Boulevard, Suite 1093
Winter Park, Florida 32792

Abstract. To the best of our knowledge, proposed is the first extreme-environment wireless pressure sensor design using a remoted single-crystal SiC chip within a pressurized capsule. A detailed theoretical analysis of the sensor system is performed, including the SiC chip's mechanical response within the pressure capsule and the pressure measurement technique's optical response based on image demagnification. The remote sensor was experimentally tested at room temperature for pressures up to 41 atm, and the sensor response is consistent with the theoretical analysis. The demonstrated sensor has a current experimental resolution of 1.17 atm with a designed maximum pressure range of 140 atm. Improved sensing resolution and range can be achieved via optimal selection of the SiC chip's dimensions and its seating in the pressure capsule. Applications for this sensor include extreme environments involving hot gases and corrosive fluids, as in power generation systems, oil field operations, and aerospace systems. © *2007 Society of Photo-Optical Instrumentation Engineers.* [DOI: 10.1117/1.2432885]

Subject terms: optical sensors; pressure sensor; extreme environments.

1 Introduction

Today, fiber-optic sensors are used in industry for various sensing applications in aircraft, locomotives, bridges, and power systems.[1] A particular industrial scenario is fossil-fuel-based power generation systems, which fall into the category of extreme environments in terms of temperature, pressure, and caustic fluids and gases. Generation of clean energy is an important global concern.[2] Early fossil-fuel power generation system designs show improved conversion efficiencies and lower greenhouse gas emissions when operating at extreme temperatures ($>1500°C$) and pressures (>50 atm).[3] These next-generation power production systems need long-lifetime high-reliability sensors for extreme temperature and pressure measurements. Most importantly, these sensors need to survive the extreme high-temperature, high-pressure chemical conditions, including corrosive fluids, hot gases, molten metals, and sludge/waste. Of particular importance are extreme-environment pressure sensors, the subject of the present paper.

Pressure sensors have been built by utilizing the variation in the resistance or capacitance of a device under pressure. Prototype silicon carbide (SiC) high-temperature piezoresistive pressure sensors were batch-fabricated at the NASA John Glenn Research Center by producing the diaphragms using a chemical micromachining process, and the sensors showed promise and were demonstrated to operate up to 500°C.[4] Okojie et al.[5] fabricated and tested piezoresistive pressure sensors at 1000 psi (68 atm) with full-scale output 40.66 and 20.03 mV at 23 and 500°C, respectively.

Ziermann et al.[6] used SiC on insulator (SiCOI) to create a piezoresistive pressure sensor and tested its operation between room temperature and 500°C. They reported the sensitivity of the device to be 20.2 μV/(V kPa) at room temperature. Since these SiC electronic sensors are based on the principle of piezoresistance, micropipe defects in SiC negatively impact performance when compared to silicon-based electronic sensors. Attempts have also been made to make SiC membrane optical microelectromechanical system (MEMS) fiber optic pressure sensors using sapphire fibers.[7] Here, performance is shown for relatively low pressures (e.g., 20 psi) using thin SiC membranes. Moreover, all these SiC MEMS pressure sensors are wired nonpassive devices. In other words, electronic power and processing is done on the front-end chip or via a remoted fiber wire (e.g., sapphire fiber, which is limited by multimodal optical noise) that is simultaneously exposed to the changing extreme environment. In effect, all the processing in the chip (plus the fiber connection for the optical MEMS case) must withstand any extreme environmental effects. Thus the packaging of the remoting wire for the sensor becomes a key concern and limitation. Hence, works were implemented to produce a wireless electronic pressure sensor.[8–10] These highlighted sensors require on-chip power plus electronics and contacts, which are nonrobust to high temperatures. Another design proposed[11] is passive, nevertheless, it presently has limitations in the temperature ($<400°C$) and pressure (<7 bars) ranges of operation. In silicon technology, p-n junction-isolated piezoresistors are used as pressure sensors for temperatures less than 175°C, and silicon-on-insulator (SOI) sensors for temperatures up to 500°C.

Other techniques have also been investigated to measure pressure. Leading fiber-optic sensors such as those using fiber Fabry-Perot interference or in-fiber Bragg gratings with wavelength-based processing also use the fiber wire for light delivery and light return, hence inherently possessing the limitations of wired devices for extreme environments.[12–19] Optically reflective[20] and interferometric[21–24] techniques have also been investigated. The interferometric techniques were based on Fabry-Perot interferometer/cavity formed by etching a glass substrate or the tip of an optical fiber and enclosing the etched volume with a silicon diaphragm. The materials in these optical devices were glass and silicon, which will melt at the high temperature environment in fossil-fuel applications. Recently further work on optical pressure sensors has been reported, but all have their limitations due to the exposure of their nonrobust sensing element and/or their connecting fibers in the extreme power generation systems environment. These are listed in Refs. 25–32 All these fiber-based optical pressure sensors are wired designs.

Recently, a hybrid fiber–free-space optics approach to sensing was put forth that exploits both the fiber-based remoting capability and the minimally invasive nature of laser-targeted light beams incident on specific sensing front-end chips.[33–35] Specifically for harsh environments, the use of single-crystal 6H SiC has been suggested to enable temperature, pressure, and gas species sensing. It is for its material robustness to chemical attack, mechanical stability, and excellent thermal and optical properties that single-crystal SiC is chosen as the base optical sensor material. There are numerous polymer types of SiC such as 3C (cubic), 2H (hexagonal), 4H (hexagonal), 6H (hexagonal), and 15R (rhombohedral). The key point to note is the high (2500°C) melting temperature of 6H SiC, which makes it ideal for extreme temperature conditions. In addition, its Young's elastic modulus, yield strength, and Poisson ratio prove it to be a mechanically robust material. These material properties make single-crystal high thickness (e.g., 300 μm) 6H SiC an ideal, reliable candidate for use in extreme environment sensors such as are needed for coal-fired power plants. Data from a recently demonstrated SiC sensor has shown successful temperature measurements from room temperature to 1000°C, with pressures from 1 to 50 atm. SiC chip refractive index and thickness measurements up to 1000°C have also been possible with nanometer-equivalent sensitivities.[36]

This paper introduces a novel wireless optical sensor design for measuring pressure within extreme environments.[37] Pressure sensing is accomplished by monitoring the spatial optical properties of a free-space laser beam retroreflected from the SiC optical chip placed in a sealed capsule interconnected with the environment undergoing pressure changes. Specifically, environmental conditions imposed on the chip cause changes in the chip's optical and mechanical properties. By detecting and processing these changes over the entire illuminated chip region, the given extreme environmental pressure conditions can be deduced. A detailed prior-art citation for pressure sensors is given to put the proposed innovation in perspective. It is highlighted that these prior-art electronic and optical sensor designs require extreme environmental protection packaging of the sensing element to prevent sensing
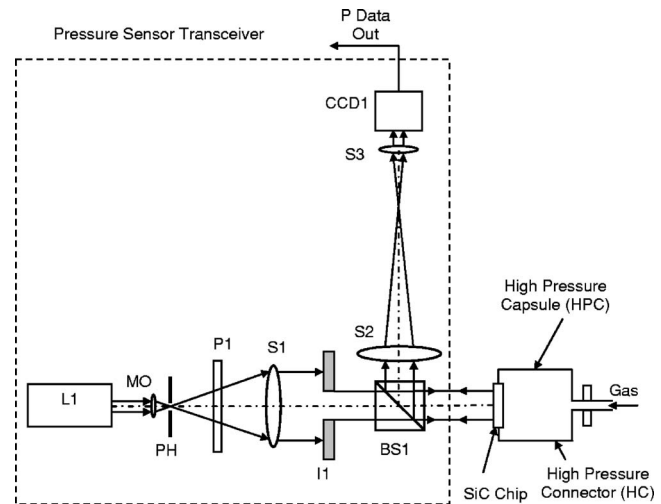

Fig. 1 Proposed SiC-chip-based wireless optical pressure sensor.

element damage, thus making a very challenging sensor design. In addition, the sensor now becomes an indirect reader of the extreme environment conditions, as it is not in direct contact with the conditions. In the proposed sensor, the SiC chip solves these prior-art problems as the SiC material itself is the direct sensing element as well as the packaging window within a basic high-pressure capsule such as one made from stainless steel or a suitable high-temperature, high-pressure ceramic. Preliminary experiments from the proposed pressure sensor are presented, including demonstrated pressure measurement ranges and sensitivity, and comparison with theoretical models for chip mechanical deformation. Issues related to sensor packaging and controls are highlighted.

2 Proposed Wireless Pressure Sensor Design

Figure 1 shows the proposed wireless pressure sensor concept that uses a remotely placed all-passive optical sensor capsule made of a single-crystal SiC chip acting as the capsule window and a pressure-sealed capsule assembly made of a suitable high-pressure, high-temperature material such as a ceramic (including SiC forms, e.g., sintered SiC) or high-pressure stainless steel. The capsule has a high-pressure connector that interfaces to a high-pressure hot gas (or fluid) flow system that is linked to the high-temperature, high-pressure hot gas flow system such as a fossil fuel plant under test. The SiC optical window sits in a specially designed, sealed pressure seat that creates the desired high-pressure boundary conditions for the deployed SiC chip.

The sensor in Fig. 1 operates as follows. The input laser beam from a laser L1 is passed through an expansion-filter system consisting of a microscope objective lens MO and pinhole PH. The cleaned and expanded beam is vertically polarized using a polarizer P1 and then collimated using a biconvex lens S1. The portion of the light beam that transmits through the beamsplitter BS1 hits the SiC chip seated in the high-pressure capsule with a sealed circular boundary. The size of the beam hitting the SiC chip is controlled by an iris I1 that is placed between S1 and BS1. Under ambient atmospheric pressure conditions (atmospheric pressure, or 1 atm), the reflections from the front and back

surfaces of the SiC chip give a phase map that represents the relative optical path length (OPL) differences between the two surfaces. This phase information is seen on a 2-D CCD detector CCD1 in the form of fringes. The initial fringe pattern can be written as $I_i(x,y)$, the initial phase map of the given SiC chip. For a perfect flatness parallel faces chip, one would not observe any fringes, just a gray-scale uniform optical power level. Imaging lenses S2 and S3 are used to form a 1:1 imaging system between the SiC chip and the CCD. For the laboratory experiments discussed later, a compressed air cylinder is connected to the pressure capsule via a manual regulator to control the pressure inside the capsule relative to the external ambient atmospheric pressure.

The key principle of operation of the proposed sensor is the global sensing of the chip deformation due to pressure. As the pressure in the capsule increases with respect to the external ambient pressure, the SiC chip undergoes a mechanical deformation and assumes a convex mirror position for the striking incident collimating beam. In effect, the SiC convex mirror acts as a diverging refractive weak lens that produces a beam expansion for the reflected incident beam. Hence, one should expect a magnification of the beam received at the remote CCD. However, given that the Fig. 1 design uses a 1 : 1 imaging system between the chip and the CCD, the chips convex-mirror-like deformation combined with the inverting imaging system produces a reduction in the beam size at the CCD with increasing pressure. Hence by monitoring the optical beam's image size on the CCD, a pressure measurement can be achieved remotely. Because CCDs are highly light-sensitive devices and single-crystal SiC is sufficiently reflective (e.g., >10% reflectivity) for visible laser wavelengths, only a low-power (e.g., <10 mW) laser is required for the proposed sensor design. Note that for highly remote distance operations (when the transceiver and capsule distances exceed, for example, 1 m), lenses S2 and S3 can be removed. In this case, the received beam expansion is monitored to access the pressure. For the present paper, the basic design in Fig. 1 is investigated as appropriate for short-distance remoting as in a controlled laboratory environment.

3 Wireless Pressure Sensor Mechanical and Optical Response

The SiC chip undergoes a mechanical deformation as the pressure in the capsule is increased. In order to evaluate the nature and extent of this deformation, a theoretical analysis of the mechanical response of the SiC chip within the pressure capsule becomes essential. The nature and extent of this mechanical response is in turn responsible for the optical response of the sensor system. Hence, for optimal pressure sensor design a mathematical relationship between the mechanical and optical responses within the sensor system needs to be established.

The mechanical response of the deployed 6H SiC chip is dependent on its mounting in the given test pressure capsule. Specifically, the mounting method defines the boundary condition necessary for solving the equations that give the amount of deflection of the SiC chip, which in turn determines the power of the pressure-sensitive convex mirror behavior of the chip. Considering the design of the chip seat, two major methods, namely, a circular chip with

Applied Uniform Differential Pressure P
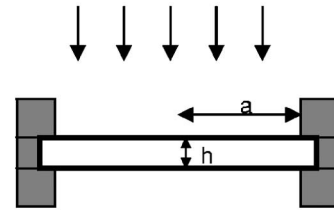
(a)

Applied Uniform Differential Pressure P
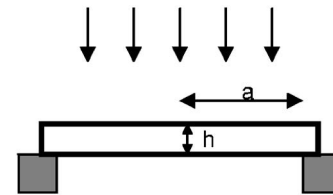
(b)

Fig. 2 The two key mechanical models, (a) clamped edge and (b) simply supported model, used to analyze the SiC chip mechanical deformation when seated in the proposed high-pressure capsule.

clamped edges and a circular chip with simply supported edges, are analyzed for the test capsule [see Fig. 2(a) and 2(b)]. In effect, the SiC chip experimental mounting method, shown later for the test capsule in this study, results in a hybrid solution of the mentioned methods.

Furthermore, the deflection analysis is subdivided under two regimes of small- and large-deflection analysis. The small-deflection regime is defined by the condition that the maximum deflection should be less than half the thickness of the chip.[38] Specifically, the region in the middle plane of the sensor chip undergoes small displacements perpendicular to the direction of the plane, thus forming the middle surface of the chip. When these displacements are small in comparison with the thickness of the chip, the strain of the middle plane can be neglected and analysis is in the small-deflection regime. When this is not true, the analysis is extended to include the effect of strain of the middle plane of the chip. This large-deflection regime analysis gives deflection and stress results that deviate from the small-deflection regime. As shown later via the experiments, the proposed pressure sensor operates well within the small-deflection regime of the utilized 6H SiC chip.

Also note that failure stress analysis of the SiC chip is essential for a robust sensor design. Hence, the maximum stress values generated for all pressure cases have to be evaluated. Proper design requires working with pressures that generate maximum stress values that are less than the failure yield stress value for 6H SiC. This pressure-limited operation ensures the reliable and repeatable performance of the SiC chip and hence the proposed wireless optical pressure sensor.

Under uniformly distributed applied pressure, a circular

sensor chip with clamped edges [see Fig. 2(a)] exhibits deflection according to the following classical expression:[38]

$$w(r) = \frac{P(a^2 - r^2)^2}{64D},$$ (1)

where $w(r)$ is the out of plane deflection in the chip at a certain radius distance r, P is the applied differential pressure between the two isolated sides of the chip, a is the radius of the chip, and D is its rigidity constant, defined as

$$D = \frac{Eh^3}{12(1 - \nu^2)},$$ (2)

where E is the chip material's modulus of elasticity, h is its thickness, and ν is its Poisson's ratio. The maximum deflection is at the center of the chip and is given by

$$w_{\max} = \frac{Pa^4}{64D}.$$ (3)

The maximum stress caused by pressure is at the boundary of the chip and is given by the equation

$$(\sigma_r)_{\max} = \frac{3Pa^2}{4h^2}.$$ (4)

For a circular sensor chip with supported edges [see Fig. 2(b)], the deflection under uniformly distributed applied pressure is given by the following expression[38]:

$$w(r) = \frac{P(a^2 - r^2)}{64D} \left(\frac{5 + \nu}{1 + \nu} a^2 - r^2 \right).$$ (5)

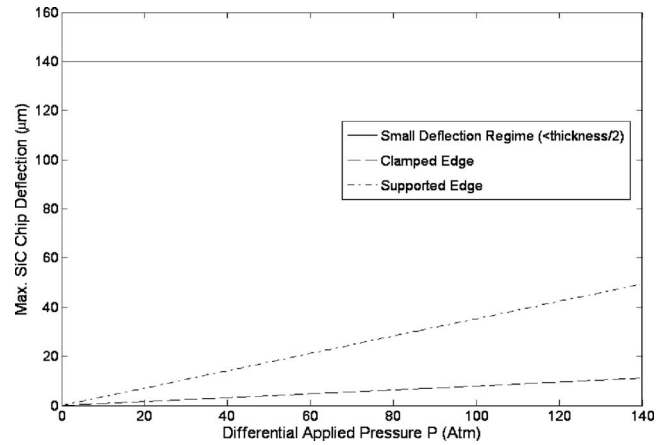The maximum deflection is at the center of the chip and is given by

$$w_{\max} = \frac{Pa^4}{64D} \left(\frac{5 + \nu}{1 + \nu} \right).$$ (6)

The maximum stress in the supported chip caused by pressure is at the center of the chip and is given by the equation

$$(\sigma_r)_{\max} = \frac{3Pa^2(3 + \nu)}{8h^2}.$$ (7)

Now consider the proposed case of a 6H SiC chip with thickness h of 280 μm, radius a of 2.5 mm, Poisson's ratio ν of 0.16, and Young's modulus E of 415 GPa.[39,40] Figure 3 shows the expected deflection produced for 6H SiC sensor chip with the applied differential pressure in the pressurized capsule. The maximum deflection of the sensor chip, with a 5-mm-diameter pressure boundary and thickness of 280 μm, is expected to be well within the small-deflection range (i.e., <thickness/2 = 140 μm) at 100 atm. The expected stress produced in the 6H SiC sensor chip with the applied differential pressure in the pressurized capsule is shown in Fig. 4. Using a 1-GPa yield stress[41] (approximate) for the 6H SiC chip, the demonstrated wireless pressure sensor is expected to work safely up to a pressure of 100 atm.

Comparing the two SiC chip seating setups of Fig. 2 in the small-deflection regime, the supported-edge chip seat-

Fig. 3 Maximum SiC chip deflection $w_{\max}$ (at the center of the chip) versus applied pressure for the clamped-edge and supported-edge boundary condition models. The chip boundary diameter was taken to be 5 mm.

ing case gives approximately 3.7 to 5 times larger deflection than the clamped chip case (see Fig. 3) but then it also gives 1.5 to 1.75 times higher maximum stress value (see Fig. 4). Since the experimental setup to seat the SiC chip in the high-pressure cell utilized in the present study is a hybrid of the two cases, the maximum stress value is expected to be in a range whose limits are defined by the stress values given by the mentioned two cases. The same discussion holds true for the maximum deflection of the SiC chip. Note that in the large-deflection regime, exact analytical solutions are not available and only approximate analytical solutions can be utilized. However, numerical methods and simulation tools (like finite element method software) can provide more exact solutions for the plate/chip deflections and stress values.

After deflection according to Eq. (1) or (5) in the small-deflection regime, the surface of the SiC chip and hence the optical response of the SiC chip can be approximated by a weak lens. Geometrical analysis for weak lensing mirror optics (i.e., when the lensing mirror radius of curvature R is
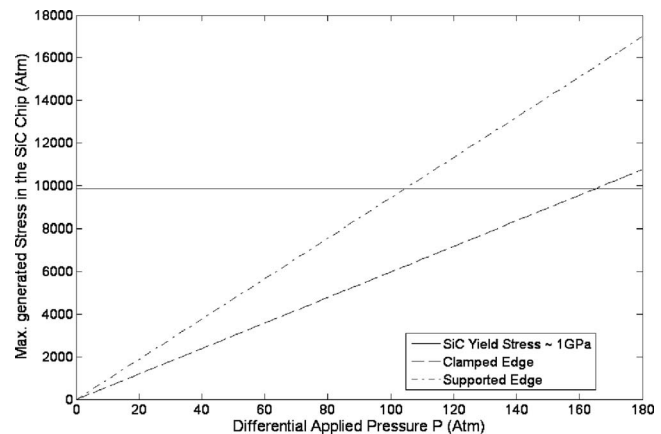
**Fig. 4** The expected stress produced in a SiC sensor chip of 5-mm diameter and 280-μm thickness.

Table 1 Theoretical central deflections and focal lengths of the SiC chip convex mirror versus pressure.

Differential pressure P		Model 1: Supported sensor chip		Model 2: Clamped sensor chip	
(psi)	(atm)	Central deflection w_{max} (μm)	Focal length f_m (cm)	Central deflection w_{max} (μm)	Focal length f_m (cm)
0	0	0.000	∞	0.000	∞
200	13.61	4.804	32.53	1.080	144.68
300	20.41	7.206	21.68	1.620	96.45
400	27.21	9.608	16.26	2.160	72.34
500	34.01	12.010	13.01	2.699	57.87
600	40.82	14.412	10.84	3.240	48.23

much less than the lensing mirror central thickness w_{max}) can be carried out to show that the focal length f_m of the SiC weak convex mirror is given by

$$f_m = \frac{R}{2} = \frac{w_{max}^2 + a^2}{4w_{max}^2 \times 10^4} \text{ cm}, \tag{8}$$

where w_{max} is the SiC chip central position maximum displacement with applied differential pressure P, and a is the radius in microns of the SiC chip pressure boundary. Using Eqs. (3), (6), and (8) and a pressure boundary of $a = 2.5$ mm, Table 1 gives the theoretically expected maximum chip central deflection and equivalent weak focal length values for the SiC chip under specific varying pressure values. These pressure values were implemented later in the experiment. In addition, Fig. 5 shows the theory-predicted focal length change for the SiC weak mirror for a broad range of pressures.
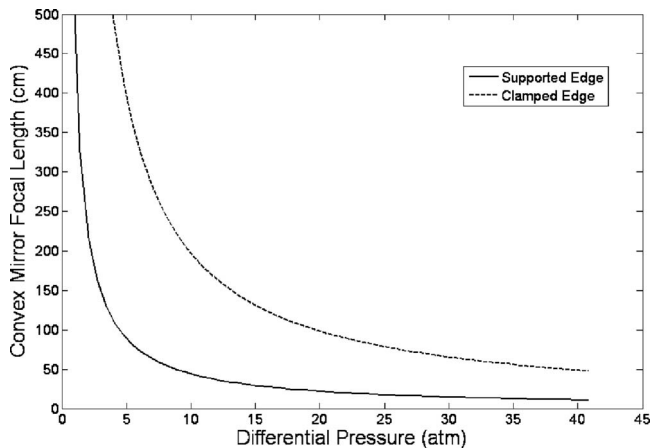
Fig. 5 Effective theoretical focal length f_m of the SiC chip acting as a convex mirror due to applied pressure. The focal length decreases as the differential pressure is increased.

Recall that the SiC chip acts as a weak convex mirror (equivalently, a weak concave lens) within the proposed (Fig. 1) wireless optical sensor setup containing the S2/S3 1:1 imaging system. The lenses S2 and S3 have focal lengths F_2 and F_3, respectively ($F_2 = F_3 = F$). When the SiC chip experiences no differential pressure ($P=0$), it acts like a flat mirror and the S3/S4 lenses form a 1:1 imaging system with magnification $M=1$. As P increases, the SiC chip starts acting like a convex mirror (or concave lens) with a long negative value focal length. It is well known that the equivalent focal length f_e for two lenses (convex lens focal length F_2 and mirror focal length f_m) placed L apart is given by[42]

$$f_e = \frac{F_2(L - f_m)}{L - (F_2 + f_m)}. \tag{9}$$

Hence, the SiC chip weak concave lens in combination with the first imaging lens S2 forms an equivalent imaging lens with a new focal length f_e. With $F_2 = F$ and $L = F$, and considering weak lensing conditions, which are true for the proposed SiC pressure sensor, the new pressure-dependent optical linear demagnification M (f_m is a negative value) for the imaging system can be approximately written as

$$M = \frac{F_3}{f_e} = \frac{F}{f_e} = \frac{f_m}{f_m - F} = \frac{1}{1 - F/f_m}. \tag{10}$$

As M can be measured by computer-based image processing of the CCD-acquired images in Fig. 1 and F is known, f_m can be calculated. Furthermore, as f_m is related to w_{max} of the SiC chip [see Eq. (8)] and w_{max} is related to the differential pressure P in the capsule [see Eqs. (3) and (6)], the measured pressure P can be calculated. As actual experimental conditions for the SiC chip seating can be a combination of the clamped and supported chip deformation models, each proposed wireless sensor should be calibrated using a state-of-the-art pressure gauge. In effect, a sensor calibration table should be deployed that stores pre-
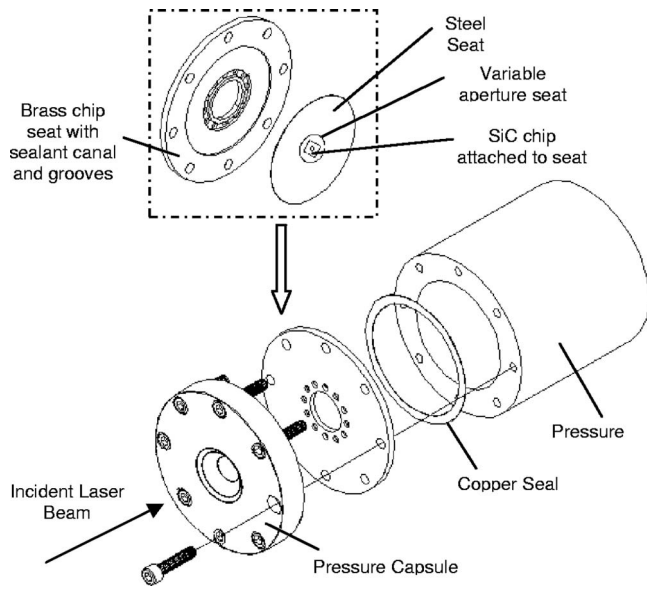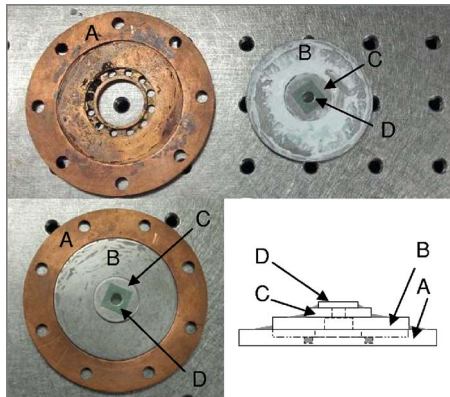
Fig. 6 Experimental design used for seating the SiC chip in the high-pressure capsule.

cision taken pressure values and their corresponding M values provided by the wireless optical pressure sensor. In this way, any nonlinear effects within the pressure versus M function can be calibrated into the sensor measurements, leading to reliable and accurate pressure measurements.

4 Wireless Pressure Sensor Demonstration

In order to study the pressure measurement aspects of the proposed wireless sensor in Fig. 1, a high-pressure stainless steel capsule is fabricated as shown in Fig. 6. Figure 7 shows the manner in which a square 1×1-cm SiC chip is seated in the pressure capsule. The variable aperture seat (washer) used has a 5-mm diameter and creates the circular pressure boundary on the chip. The washer is attached to the steel seat by a GE RTV 102 silicone rubber adhesive sealant with operational temperature range of -60 to $204 °C$. The SiC chip is attached to the washer us-


Fig. 7 Snapshot of the experimental seating components and their arrangements used for seating the 6H SiC chip in the high-pressure capsule. Components in photograph are labeled as follows: A, brass chip seat holder with sealant canal and grooves; B, steel seat; C, aperture seat (washer), and D, SiC chip.

ing a layer of the same sealant. The sealant is filled in the canal of the brass seat so it strongly holds onto the steel seat. A layer of the sealant was also applied at the edges of the two seats to avoid any leaks. Note that for high-temperature or temperature-independent pressure sensor operation, a modified SiC seating design should be utilized to match the seat and chip material's thermal coefficient of expansion (CTE) values to avoid temperature-dependent global chip deformation. This aspect will be pursued in future advanced-stage work.

To enable the present sensor design of Fig. 1, a 10-mW 633-nm (red wavelength) linear-polarization He–Ne laser is used as the source L1. The expansion-filter system utilizes a $10 \times$ MO lens and a 10-μm PH. The collimating lens has a focal length of 15 cm. The sealed circular boundary of the SiC chip for the experiment is of $\approx$5-mm diameter. Imaging lenses S2 and S3 have 10-cm focal lengths, forming a 40-cm-path $1 : 1$ imaging system between the SiC chip and the CCD. The temperature condition during the experiment is the ambient $26 °C$ room temperature. The manual regulator connected to the compressed air cylinder is used to control the pressure inside the capsule relative to the external ambient 1-atm pressure.

As shown in Fig. 8, as the pressure in the capsule increases above 1 atm, the differential pressure P on the SiC chip produces an increasing convex-mirror chip deformation of the initial pattern $I_i(x, y)$, thus producing a pattern reduction in size. Figure 8 shows the set of images from the wireless pressure sensor where the initial fringe pattern size decreases with increasing capsule differential pressures up to 40.8 atm (1 psi=0.068 atm). A quantization of the image reduction versus applied differential pressure P in the capsule for P taken up to 40.8 atm is shown in Table 2, giving the experimentally measured values for M versus P. Figure 9 connects the discrete experimental data to show a plot of differential pressure P on SiC chip versus image size given by pixel count. These results show a linear behavior of the applied differential pressure P versus the measured optical parameter of image size. The sensor pressure resolution is given by the inverse of the slope of the plot in Fig. 9. This plot indicates a current experimental resolution of 1.17 atm, calculated as 40.82 atm/$[(147-112)$ pixels$]$. The resolution measurement is restricted by the pixel size in the deployed CCD. Here 147 pixels of the CCD $=$ 5 mm real size using the $1 : 1$ imaging approach. One can greatly improve the pressure measurement resolution by decreasing the pixel size and increasing the size of the optical beam on the CCD plane. This is to our knowledge the first demonstration of a wireless SiC optical chip for high-pressure assessment and points to the robustness of the thick SiC chip under high gas pressures, a result needed for potential fossil-fuel power generation system gas species detection using custom SiC chips. For comparison and sensor design accuracy, Fig. 10 shows plots for the experimentally detected image magnification M versus pressure P for the studied wireless sensor versus the theoretical design plots. These plots indicate that the SiC chip seating is closer to the clamped case, an expected results because of the pressure washer (seal) used to maintain the chip in a sealed arrangement. In addition, the results in Fig. 10 indicates linear operation of the demonstrated pressure sensor, with
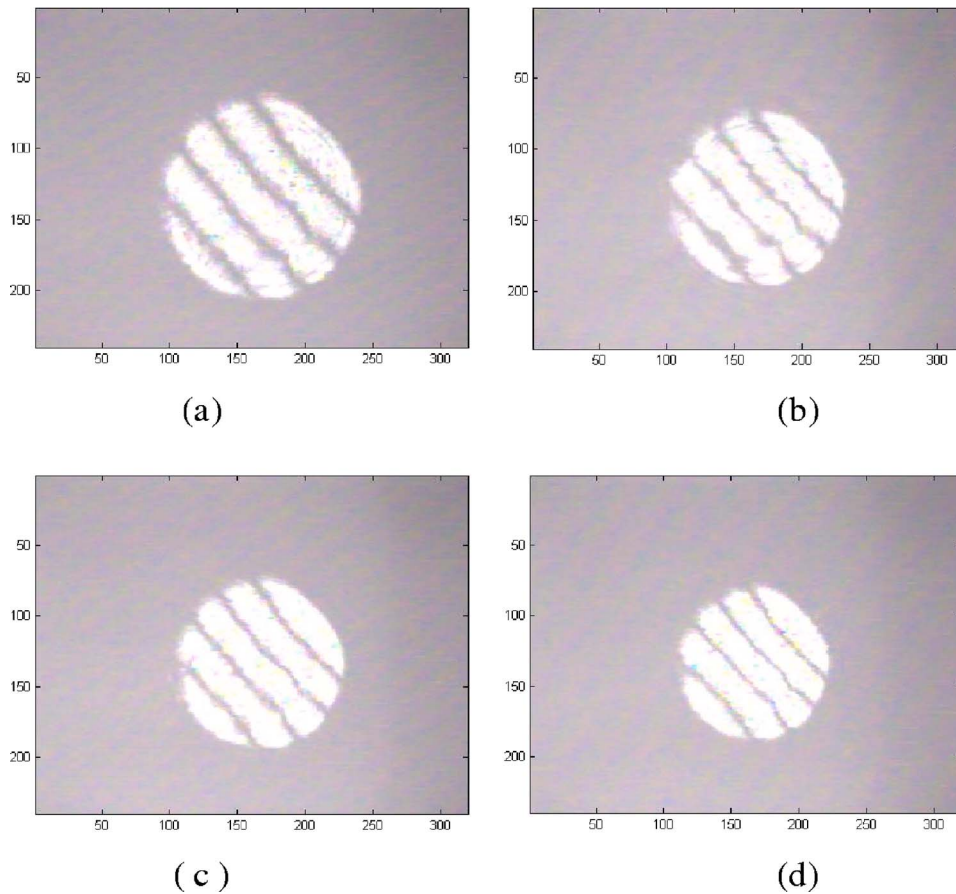
Fig. 8 Optical images $I_i(x, y)$ produced by the SiC-chip-based pressure system for (a) 0 atm, (b) 13.6 atm (200 psi), (c) 27.2 atm (400 psi), and (d) 40.8 atm (600 psi) high differential pressure conditions in the pressure capsule. Dimensions on both axes are in CCD pixels.

the SiC chip performance well within the linear elastic small-deformation range, a need for long-life repeatable robust sensor operations.
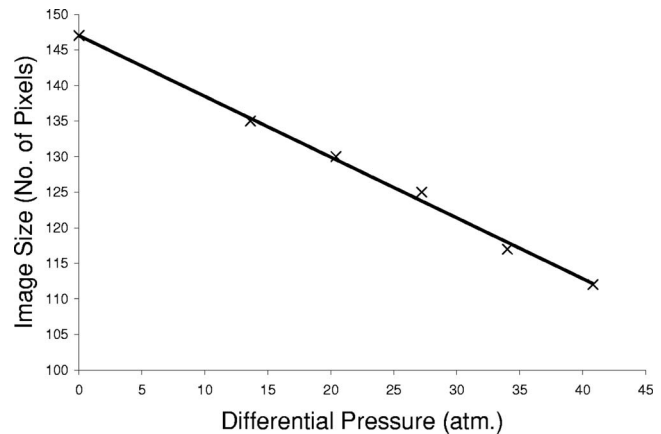
5 Conclusion

An extreme-environment wireless pressure sensor design has been proposed, using a thick single-crystal 6H SiC chip seated in a pressure capsule that can be designed for extreme conditions. The sensor operates on the principle of remote laser beam targeting, SiC chip optical weak lensing, and received-beam image measurement. The concept has been tested up to 41 atm with an initial 1.17-atm pressure measurement resolution. Experimental results also show a

Table 2 Experimental optical image size versus capsule differential pressure P.

Differential pressure P		Image size	Measured magnification
(psi)	(atm)	(CCD pixels)	M = image size/147
0	0	147	1.00
200	13.61	135	0.92
300	20.41	130	0.88
400	27.21	125	0.85
500	34.01	117	0.80
600	40.82	112	0.76

Fig. 9 Plot of demagnification of incident beam as it reflects from the SiC chip under pressure acting as a weak convex mirror coupled to a 1:1 image inversion system.
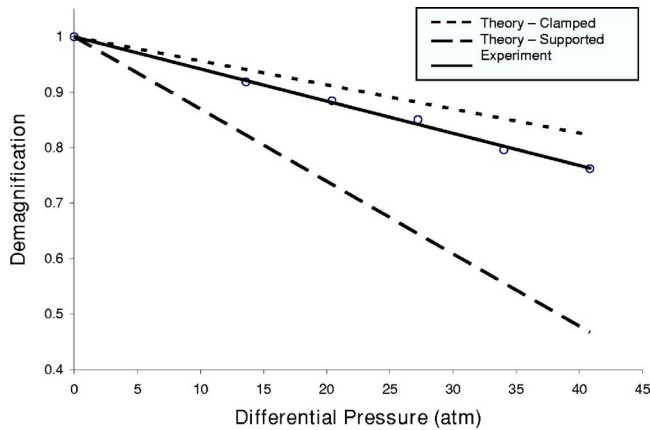
Fig. 10 Experimental beam demagnification along with the theoretical demagnification for clamped and supported sensor chip models. The behavior of the chip shifts from the clamped model towards the supported model as the pressure increases.

linear mechanical and optical behavior of the SiC chip and sensor demagnification parameter readout, indicating the expected robustness of the SiC chip technology under high pressures. Mechanical deflection analysis points to a clamped seating case for the SiC chip within the capsule, while chip stress analysis indicates a robust design reaching 140 atm and beyond. The sensor resolution can be improved with optimized SiC chip and capsule designs. These initial results attest to the promise and strengths of SiC-chip-based optical wireless sensor technology for fossil-fuel–based power generation system applications. Future work relates to designing a temperature-independent wireless pressure sensor with optimal capsule packaging and extensions to long-distance remote sensor operations.

References

1. B. Culshaw, "Fiber-optic sensors: applications and advances," *OSA Opt. Photon. News* **16**, pp. 24–29 (Nov. 2005).
2. P. Fairley, "The greening of GE," *IEEE Spectrum* **42**(7), pp. 28–33 (July 2005).
3. J. H. Ausubel, "Big green energy machines," *Ind. Phys.* **10**(5), pp. 20–24, (Oct.-Nov. 2004).
4. R. S. Okojie, A. A. Ned, and A. D. Kurtz, "Operation of α(6H)-SiC pressure sensor at 500°C," in *IEEE int. Con. on Solid-State Sensors and Actuators*, pp. 1407–1409 (1997).
5. R. S. Okojie, A. A. Ned and A. D. Kurtz, "Operation of α(6H)-SiC pressure sensor at 500°C," *Sens. Actuators, A* **66**(1–3), 200–204 (1998).
6. R. Ziermann, J. von Berg, W. Reichert, E. Obermeier, M. Eickhoff, and G. Krötz, "A high temperature pressure sensor with β-SiC piezoresistors on SOI substrates," in *IEEE Int. Con. on Solid-State Sensors and Actuators*, pp. 1411–1414 (1997).
7. W. Pulliam, P. Russler, R. Mlcak, K. Murphy, and C. Kozikowski, "Micromachined SiC fiber-optic pressure sensors for high temperature aerospace applications," *Proc. SPIE* **4202**, 21–30 (Dec. 2000).
8. A. Dehennis and K. D. Wise, "A double-sided single-chip wireless pressure sensor," in *15th IEEE Int. Con. on MEMS*, pp. 252–255. (2002).
9. O. Akar, T. Akin, and K. Najafi, "A wireless batch sealed absolute capacitive pressure sensor," in *14th Eur. Con. on Solid State Transducers (EuroSensors)*, pp. 585–588 (2000).
10. G. Schimetta, F. Dollinger, and R. Weigel, "A wireless pressure-measurement system using a SAW hybrid sensor," *IEEE Trans. Microwave Theory Tech.* **48**, 2730–2735 (Dec. 2000).
11. M.A. Fonseca, J. M. English, M. von Arx, and M. G. Allen, "Wireless micromachined ceramic pressure sensor for high-temperature applications," *J. Microelectromech. Syst.* **11**, 337–343 (2002).
12. C. E. Lee and H. F. Taylor, "Sensors for smart structures based on the Fabry-Perot interferometer," Chap. 9, *Fiber Optic Smart Structures*, Eric Udd, Ed. pp. 249–270 Wiley, New York, 1995.
13. R. Duncan, D. Gifford, and V. Rajendran, "OFDR tracks temperatures on power generators," *Laser Focus World Mag.* **39**(1010), 89–92, (2003).
14. A. D. Kersey, M. A. Davis, H. J. Patrick, M. LeBlanc, K. P. Koo, C. G. Askins, M. A. Putnam, and E. J. Friebele, "Fiber grating sensors," *J. Lightwave Technol.* **15**(8), 1442–1463 (1997).
15. B. Culshaw, "Optical fiber sensor technologies: opportunities and perhaps pitfalls," *J. Lightwave Technol.* **22**(1), 39–50 (2004).
16. L. Tenerz, L. Smith, and B. Hök, "A fiber optic silicon pressure microsensor for measurements in coronery arteries," in *Proc. Sixth Int. Conf. on Solid State Sensors and Actuators, Digest of Technical Papers, Transducers'91*, pp. 1021–1023 (1991).
17. R. A. Wolthuis, G. L. Mitchell, E. Saaski, J. C. Harti, and A. Afromowitz, "Development of medical pressure and temperature sensors employing optical spectrum modulation," *IEEE Trans. Biomed. Eng.* **38**, 974–981 (1991).
18. Y. Kim and D. P. Neikirk, "Micromachined Fabry-Perot cavity pressure transducer," *IEEE Photonics Technol. Lett.* **7**(12), 1471–1473 (1995).
19. J. Han, J. Y. Kim, T. S. Kim, and J. S. Kim, "Performance of Fabry-Perot microcavity structures with corrugated diaphragms," *Sens. Actuators, A* **79** 162–172 (2000).
20. T. Katsumata, Y. Haga, K. Minami, and E. Esashi, "Micromachined 125 μm diameter ultra-miniature fiber-optic pressure sensor for catheter," *Trans. Inst. Electr. Eng. Jpn., Sect. E* **120**, 58–63 (2000).
21. J. Zhou, S. Dasgupta, H. Kobayashi, J. M. Wolff, H. E. Jackson, and J. T. Boyd, "Optically interrogated MEMS pressure sensors for propulsion applications," *Opt. Eng.* **40**, 598–604 (2001).
22. D. C. Abeysinghe, S. Dasgupta, J. T. Boyd, and H. E. Jackson, "A novel MEMS pressure sensor fabricated on an optical fiber," *IEEE Photonics Technol. Lett.* **13**, 993–995 (2001).
23. W. Li, D. C. Abeysinghe, and J. T. Boyd, "Wavelength multiplexing of microelectromechanical system pressure and temperature sensors using fiber Bragg gratings and arrayed waveguide gratings," *Opt. Eng.* **42**(2), 431–438 (2003).
24. W. J. Wang, R. M. Lin, D. G. Guo, and T. T. Sun, "Development of a novel Fabry-Perot pressure microsensor," *Sens. Actuators, A* **116**(1), 59–65 (2004).
25. W. Li, D. C. Abeysinghe, and J. T. Boyd, "Multiplexed sensor system for simultaneous measurement of pressure and temperature," *Opt. Eng.* **43**(1), 148–156 (2004).
26. D. Guo, W. Wang, and R. Lin, "Theoretical analysis and measurement of the temperature dependence of a micromachined Fabry-Perot pressure sensor," *Appl. Opt.* **44**(2), 249–256 (2005).
27. Y. Zhu and A. Wang, "Miniature fiber-optic pressure sensor," *IEEE Photonics Technol. Lett.* **17**(2), 447–449 (2005).
28. J. Xu, G. Pickrell, X. Wang, W. Peng, K. Cooper, and A. Wang, "A novel temperature insensitive optical fiber pressure sensor for harsh environments," *IEEE Photonics Technol. Lett.* **17**(4), 870–872 (2005).
29. D. Donlagic and E. Cibula, "All-fiber high sensitivity pressure sensor with SiO$_2$ diaphragm," *Opt. Lett.* **30**(16), 2071–2073 (2005).
30. H. Xiao, J. Deng, Z. Wang, W. Huo, P. Zhang, M. Luo, G. Pickrell, R. May, and A. Wang, "Fiber optic pressure sensor with self-compensation capability for harsh environment applications," *Opt. Eng.* **44**(5), 054403 (2005).
31. M. Li, M. Wang, and H. Li, "Optical MEMS pressure sensor based on Fabry-Perot interferometry," *Opt. Express* **14**(4), 1497–1504 (2006).
32. Y. Zhu, K. L. Cooper, G. R. Pickrell, and A. Wang, "High-temperature fiber-tip pressure sensor," *J. Lightwave Technol.* **24**(2), 861—869 (2006).
33. N. A. Riza, M. A. Arain, and F. Perez, "Harsh environments minimally invasive optical sensing technique for extreme temperatures: 1000°C and approaching 2500°C," *Proc. SPIE* **5855**, 687–690 (2005).
34. N. A. Riza, M. A. Arain, and F. Perez, "Harsh environments minimally invasive optical sensor using freespace targeted single crystal silicon carbide," *IEEE Sens. J.* **6**(3), 672–675 (2006).
35. M. A. Arain and N. A. Riza, "Fiber coupled in-line heterodyne opti-

cal interferometer for minimally invasive sensing," *J. Lightwave Technol.* **23**(8), 2449–2454 (2005).

36. N. A. Riza, M. Arain, and F. Perez, "6-H single crystal silicon carbide thermo-optic coefficient measurements for ultrahigh temperatures upto 1273 K in the telecommunications infrared band," *J. Appl. Phys.* **98**(10), 103512 (2005).

37. N. A. Riza, F. N. Ghauri, and F. Perez, "Hybrid optical sensor using laser targeting," in *Optical Sensing II*, B. Culshaw and A. Mignani, Eds. *Proc. SPIE* **6189** (2006).

38. S. P. Timoshenko and S. Woinowsky-Krieger, *Theory of Plates and Shells*, Chap. 2, pp. 56–57, McGraw-Hill, New York (1959).

39. NIST Structural Ceramic Data Base, SRD Data Base No. 30, www.ceramics.nist.gov/srd/summary/scdscs.htm

40. R. G. Munro, "Material properties of a sintered alpha-SiC," *J. Phys. Chem. Ref. Data* **26**, 1195–1203 (1997).

41. W. N. Sharpe, O. Jadaan, G. M. Beheim, G. D. Quinn, and N. N. Nemeth, "Fracture strength of silicon carbide micro-specimens," *IEEE J. Microelectromech. Sys.* **14**(5), 903–913 (2005).

42. E. Hecht, *Optics*, 2nd ed., Eq. (5.36), p. 148, Addison-Wesley, Reading, MA (1990).

Biographies and photographs of the authors not available.